The *Medicago truncatula* DMI1 Protein Modulates Cytosolic Calcium Signaling[1][W][OA]

Edgar Peiter, Jongho Sun, Anne B. Heckmann, Muthusubramanian Venkateshwaran, Brendan K. Riely, Marisa S. Otegui, Anne Edwards, Glenn Freshour, Michael G. Hahn, Douglas R. Cook, Dale Sanders, Giles E.D. Oldroyd, J. Allan Downie, and Jean-Michel Ané*

Biology Department, University of York, York YO10 5YW, United Kingdom (E.P., D.S.); John Innes Centre, Norwich Research Park, Norwich NR4 7UH, United Kingdom (J.S., A.B.H., A.E., G.E.D.O., J.A.D.); Department of Agronomy (M.V., J.-M.A.) and Department of Botany (M.S.O.), University of Wisconsin, Madison, Wisconsin 53706; Department of Plant Pathology, University of California, Davis, California 95616 (B.K.R., D.R.C.); and Complex Carbohydrate Research Center, University of Georgia, Athens, Georgia 30602–4712 (G.F., M.G.H.)

In addition to establishing symbiotic relationships with arbuscular mycorrhizal fungi, legumes also enter into a nitrogen-fixing symbiosis with rhizobial bacteria that results in the formation of root nodules. Several genes involved in the development of both arbuscular mycorrhiza and legume nodulation have been cloned in model legumes. Among them, *Medicago truncatula DMI1* (*DOESN'T MAKE INFECTIONS1*) is required for the generation of nucleus-associated calcium spikes in response to the rhizobial signaling molecule Nod factor. *DMI1* encodes a membrane protein with striking similarities to the *Methanobacterium thermoautotrophicum* potassium channel (MthK). The cytosolic C terminus of DMI1 contains a RCK (regulator of the conductance of K^+) domain that in MthK acts as a calcium-regulated gating ring controlling the activity of the channel. Here we show that a *dmi1* mutant lacking the entire C terminus acts as a dominant-negative allele interfering with the formation of nitrogen-fixing nodules and abolishing the induction of calcium spikes by the G-protein agonist Mastoparan. Using both the full-length DMI1 and this dominant-negative mutant protein we show that DMI1 increases the sensitivity of a sodium- and lithium-hypersensitive yeast (*Saccharomyces cerevisiae*) mutant toward those ions and that the C-terminal domain plays a central role in regulating this response. We also show that DMI1 greatly reduces the release of calcium from internal stores in yeast, while the dominant-negative allele appears to have the opposite effect. This work suggests that DMI1 is not directly responsible for Nod factor-induced calcium changes, but does have the capacity to regulate calcium channels in both yeast and plants.

Nitrogen and phosphorus are essential macronutrients that frequently limit plant growth. To meet their phosphorus requirements many plants undergo symbiotic interactions with arbuscular mycorrhizal fungi. In addition, leguminous plants also establish a mutualistic symbiotic interaction with rhizobial bacteria that results in the formation of root nodules wherein atmospheric nitrogen is fixed by the bacteria and transferred to the plant.

The rhizobium-legume symbiosis is initiated by the production of bacterial lipochitooligosaccharidic signals, termed Nod factors, that are produced in response to flavonoids exuded by legume roots. The perception of Nod factors initiates downstream responses, such as specific ion fluxes, root hair deformations, and induction of *EARLY NODULATION* (*ENOD*) genes (Oldroyd and Downie, 2004). Similarly, diffusible Myc factors are able to elicit symbiotic responses in host plants but the structures of these signals are unknown. Within 1 to 2 min of Nod factor application, a transient increase in cytosolic free calcium ($[Ca^{2+}]_{cyt}$) is detectable in root hair cells (Felle et al., 2000). This Ca^{2+} transient has been shown to depend on Ca^{2+} influx through the plasma membrane and is localized to the root hair tip (Shaw and Long, 2003). Following this initial $[Ca^{2+}]_{cyt}$ transient, repetitive nucleus-associated Ca^{2+} oscillations are observed in the cytosol (Erhardt et al., 1996; Walker et al., 2000). It has been shown in a number of plant and animal systems that Ca^{2+} oscillations encode information that can be translated into downstream responses (Dolmetsch et al., 1998; Allen et al., 2001) and there is also evidence that Ca^{2+} spiking is relevant for the activation of downstream responses in nodulation signaling (Miwa et al., 2006; Sun et al., 2007).

[1] This work was supported by a Hatch grant (University of Wisconsin, Madison; to J.M.A.), the Biotechnology and Biological Sciences Research Council (to J.A.D., G.E.D.O., and D.S.), a European Union Marie Curie training network grant (grant no. RTN–CT–2003–505227 to J.A.D. and A.B.H.), a David Phillips fellowship from the Biotechnology and Biological Sciences Research Council (to G.E.D.O.), and a grant from the U.S. Department of Energy Biosciences Program (grant no. DE–FG02–01ER15200 to D.R.C.).

* Corresponding author; e-mail jane@wisc.edu.

The author responsible for distribution of materials integral to the findings presented in this article in accordance with the policy described in the Instructions for Authors (www.plantphysiol.org) is: Jean-Michel Ané (jane@wisc.edu).

[W] The online version of this article contains Web-only data.

[OA] Open Access articles can be viewed online without a subscription.

www.plantphysiol.org/cgi/doi/10.1104/pp.107.097261

Since Ca^{2+} spiking appears to be a crucial component of the nodulation process, we were interested in how the Ca^{2+} signal is generated. $[Ca^{2+}]_{cyt}$ elevations are mediated by the activation of Ca^{2+}-permeable channels in membranes delineating compartments of higher $[Ca^{2+}]$. In contrast to animals, the molecular identity of Ca^{2+}-permeable channels is largely unknown in plants. The sole exception is the *TPC1* (two-pore channel) gene, encoding a Ca^{2+}-activated and Ca^{2+}-permeable channel in the vacuolar membrane (Peiter et al., 2005b). Because Nod factor-induced Ca^{2+} spiking is confined to the perinuclear area, TPC1 is not likely to be involved in this response. Genes for Ca^{2+}-permeable channels in the plant endoplasmic reticulum (ER) or nuclear envelope have not been identified, but biochemical and biophysical studies on fractionated membranes have revealed a number of Ca^{2+} conductances: Similar to the situation in some animals cells, Ca^{2+}-permeable channels in the ER can be activated by cADP Rib (Navazio et al., 2001) and inositol 1,4,5-trisphosphate ($InsP_3$; Muir and Sanders, 1997). Also, the NADP metabolite nicotinic acid adenine dinucleotide phosphate has been demonstrated to release Ca^{2+} from plant ER-derived vesicles (Navazio et al., 2000). In addition, a voltage-dependent, Ca^{2+}-sensitive, and Ca^{2+}-selective channel has been identified in ER-derived membranes from *Bryonia* tendrils (Klüsener et al., 1995). However, such in vitro studies are unable to determine whether these conductances are actually present in the nuclear envelope, which is part of the ER fraction.

Although the molecular identities of the components that make up the Ca^{2+} oscillator in the Nod factor-stimulated root hair are not known, pharmacological studies have provided some information on the mechanism of oscillations. Two inhibitors of $InsP_3$-activated channels, TMB-8 and 2-APB, inhibited expression of *ENOD11* (Charron et al., 2004), and 2-APB also blocked Ca^{2+} spiking (Engstrom et al., 2002). Recent reports that the G-protein agonist Mastoparan and its synthetic analog Mas7 activate Ca^{2+} oscillations and nodulation gene expression in a manner analogous to Nod factor-induced responses support the notion that Ca^{2+} spiking may involve phospholipid signaling (Charron et al., 2004; Sun et al., 2007). Evidence for the contribution of type II_A ATPases in the Ca^{2+} spiking response stems from experiments demonstrating a block of the response by the specific inhibitor cyclopiazonic acid (Engstrom et al., 2002). The most likely scenario is therefore a release of Ca^{2+} from the nucleus-associated compartment by ligand-activated channels followed by Ca^{2+} retrieval by type II_A Ca^{2+} pumps.

Forward genetic studies in model legumes, such as *Medicago truncatula* and *Lotus japonicus*, have revealed genes that are required for both legume nodulation and Nod factor signaling. Among them, the *DMI* (*DOESN'T MAKE INFECTIONS*) genes play a very early role in Nod factor signaling and are also necessary for the establishment of arbuscular mycorrhization, indicating a common signaling pathway. *dmi1* mutants are affected in many responses to Nod factors and particularly in the Nod factor-induced Ca^{2+} spiking response (Wais et al., 2000). Cloning of *DMI1* revealed that it encodes a putative ion channel with strong homologies to the MthK Ca^{2+}-gated K^+ channel (Ané et al., 2004). However, in contrast to the MthK channel, the putative filter region of the DMI1 protein does not contain the GYGD motif found in K^+-selective channels, leaving open the possibility that DMI1 may constitute a ligand-activated Ca^{2+} channel. In favor of this idea, DMI1 contains a regulator of the conductance of K^+ (RCK) domain that may be involved in the binding of Ca^{2+} and/or other unknown ligands (Jiang et al., 2002). Subsequently, two proteins homologous to DMI1 were identified from *L. japonicus*: CASTOR and POLLUX (Imaizumi-Anraku et al., 2005). Unexpectedly, fusions of both proteins with GFP revealed localization to plastids in onion (*Allium cepa*) cells and pea (*Pisum sativum*) roots, which is difficult to reconcile with an involvement in nucleus-associated Ca^{2+} spiking. However, it has recently been demonstrated for DMI1 that this protein is localized in the nuclear envelope (Riely et al., 2007). The fact that DMI1 is essential for Nod factor-induced Ca^{2+} spiking and localizes to the nuclear envelope around which the major Ca^{2+} changes occur made it a strong candidate for playing a direct role in the formation of Ca^{2+} spikes. Analysis of *dmi1* mutants, however, suggested that DMI1 is not required for Mastoparan-induced Ca^{2+} spiking and *ENOD11* expression (Charron et al., 2004; Sun et al., 2007). Because Mastoparan and Nod factor are likely to activate the same Ca^{2+} oscillatory mechanism, DMI1 is unlikely to function as the Ca^{2+} channel directly mediating Nod factor-induced Ca^{2+} oscillations.

To elucidate the role of DMI1 in Nod factor signaling we extended the analysis of *dmi1* mutant alleles. Here we show that *dmi1-2*, a nod mutant that lacks the entire C terminus (including the RCK domain) but maintains the full channel domain, appears to act as a dominant-negative allele. Our first indication of this was the finding that *dmi1-2* inhibits Mas7-induced Ca^{2+} oscillations. We have validated the dominant-negative nature of *dmi1-2* by showing that this allele interferes in the ability of wild-type *DMI1* to activate appropriate nodulation. To understand better the function of DMI1, we used yeast (*Saccharomyces cerevisiae*) as a heterologous expression system. When expressed in yeast, *DMI1* and *dmi1-2*, respectively, induce hypersensitivity and hypertolerance to high Li^+ and Na^+ concentrations. The notion that this phenotype is caused by altering intracellular Na^+ and Li^+ sensitivity rather than ion accumulation is supported by the facts that DMI1 is targeted to the yeast ER and that both the full-length and the truncated protein alter a Li^+-sensitive hexose-induced $[Ca^{2+}]_{cyt}$ transient originating from internal stores. The combination of mutant analysis and heterologous expression in this study provides further evidence that DMI1 is unlikely to function as an oscillatory Ca^{2+} channel, and demonstrates that DMI1 has the capacity to regulate Ca^{2+}

release channels in both yeast and plants. We hypothesize that DMI1 may function in symbiosis signaling by regulating Ca^{2+} channel activity following Nod factor and Myc factor perception.

RESULTS

dmi1-2 Suppresses Mas7-Induced Calcium Oscillations

The G-protein agonist Mastoparan, which originates from wasp venom, and its synthetic analog Mas7 have been shown to induce Ca^{2+} oscillations and nodulation gene expression in *M. truncatula* root hair cells in a manner analogous to Nod factor-induced responses (Pingret et al., 1998; Sun et al., 2007). Mas7-induced Ca^{2+} oscillations and gene induction do not require *NFP* (Nod factor perception), *DMI1*, or *DMI2* that are necessary for Nod factor-induced Ca^{2+} spiking (Charron et al., 2004; Sun et al., 2007). We undertook a more detailed analysis of Mas7 induction of Ca^{2+} spiking in all *DMI1* mutant alleles characterized to date. *dmi1-4* contains an 18 kb deletion that removes the *DMI1* promoter and a large portion of the gene. No *DMI1* transcript is expressed in this mutant that therefore represents a null allele (Ané et al., 2004; C. Rogers and G.E.D. Oldroyd, unpublished data). This mutant allele shows Mas7-induced Ca^{2+} oscillations (Fig. 1B), indicating that *DMI1* is not necessary for Mas7 induction of Ca^{2+} spiking. This is consistent with what we have shown in earlier studies using the *dmi1-1* allele (Sun et al., 2007) that contains a premature stop codon within the RCK domain (Fig. 1A). In addition, we saw Mas7-induced Ca^{2+} oscillations in the *dmi1-3* allele that contain a premature stop codon within the channel region (Fig. 1, A and B). Surprisingly, in the *dmi1-2* mutant Mas7-induced Ca^{2+} spiking was not observed (Fig. 1B), suggesting that this allele was interfering with the Mas7 mode of action. *dmi1-2* contains a premature stop codon soon after the last transmembrane domain of the channel region, thus the mutant protein should have a complete channel domain, but will lack the entire cytosolic C terminus including the RCK domain. This mutation does not affect the transcript level (Supplemental Fig. S3). Since the RCK domain represents the regulatory component of the MthK channel, we hypothesize that the product of *dmi1-2* may represent an unregulated channel. The fact that *dmi1-2* could suppress Mas7 action indicated that this mutation may act as a dominant-negative allele.

dmi1-2 Interferes with *DMI1* during Nodule Development

To assess further the effect of *dmi1-2* we attempted complementation of this mutant with the wild-type gene. Transformation of *DMI1* under the control of its native promoter and inoculation with *Sinorhizobium meliloti* led to nodule formation in hairy roots of both the *dmi1-4* and *dmi1-2* mutants (Table I). The transformed roots of the *dmi1-2* mutant produced about half as many nodules as those on the *dmi1-4* mutant; this was due to a decrease (from 90% to 70%) in the numbers of transformed roots producing nodules and a decrease (of about 40%) in the numbers of nodules formed on those roots that did produce nodules. Furthermore, there was a mixed population of nodules on complemented *dmi1-2* roots, with most nodules being white and appearing ineffective, although occasionally pink nodules did form (Fig. 2A). In contrast, complemented *dmi1-4* roots predominantly had pink nodules. We separately analyzed acetylene reduction in pink and white nodules from the complemented *dmi1-2* plants. Overall, acetylene reduction was greatly reduced in complemented *dmi1-2* compared with complemented *dmi1-4* roots (Fig. 2B) and the frequency of nodules capable of reducing acetylene was also much lower with the complemented *dmi1-2* roots (Fig. 2B). Microscopy of white nodules on complemented *dmi1-2* roots revealed that these nodules predominantly lacked bacteroids within the cells of the nitrogen-fixing zone of the nodule (Fig. 2, C and E), but did show swollen infection threads containing many bacteria (asterisk in Fig. 2E). In contrast, the few pink nodules on complemented *dmi1-2* plants were able to reduce acetylene and showed many infected plant cells (arrow in Fig. 2D) and normal bacteroid development (Fig. 2F). Complemented *dmi1-4* plants showed mostly normal nodule development with appropriate bacterial release and bacteroid development (data not shown). Based on the fact that *dmi1-2* interferes with Mas7-induced Ca^{2+} spiking and cannot be fully complemented by *DMI1* we conclude that *dmi1-2* probably acts as a dominant-negative allele with the capacity to interfere with Ca^{2+} release in plant cells.

DMI1 Exacerbates the Sensitivity of a Na^+- and Li^+-Sensitive Yeast Mutant

Because it was difficult to infer a function of DMI1 from in planta studies, we chose to express *DMI1* in a heterologous system. Budding yeast has been successfully used in the past to characterize plant ion channels and transporters. As DMI1 shares strong homology to cation channels, we expressed *DMI1* in yeast mutants defective in cation homeostasis.

The *cch1*Δ*mid1*Δ mutant is unable to grow on Ca^{2+}-depleted media because it lacks a plasma membrane Ca^{2+} channel (Fischer et al., 1997), whereas the *trk1*Δ*trk2*Δ*tok1*Δ mutant requires high K^+ concentrations in the medium due to the lack of high-affinity K^+ uptake systems (Bertl et al., 2003). Expression of *DMI1* did not suppress the phenotypes of either strain (Supplemental Fig. S1).

Unlike plant cells, wild-type yeast tolerates very high levels of Na^+ in the medium. This is mainly due to the presence of four Na^+/Li^+ pumps, ENA1 to ENA4, in the yeast plasma membrane, facilitating a highly efficient removal of Na^+ and Li^+ from the cytosol (Quintero et al., 1996). Accordingly, an *ena1*Δ-*ena4*Δ deletion mutant, G19, is hypersensitive to Na^+ and Li^+ (Quintero

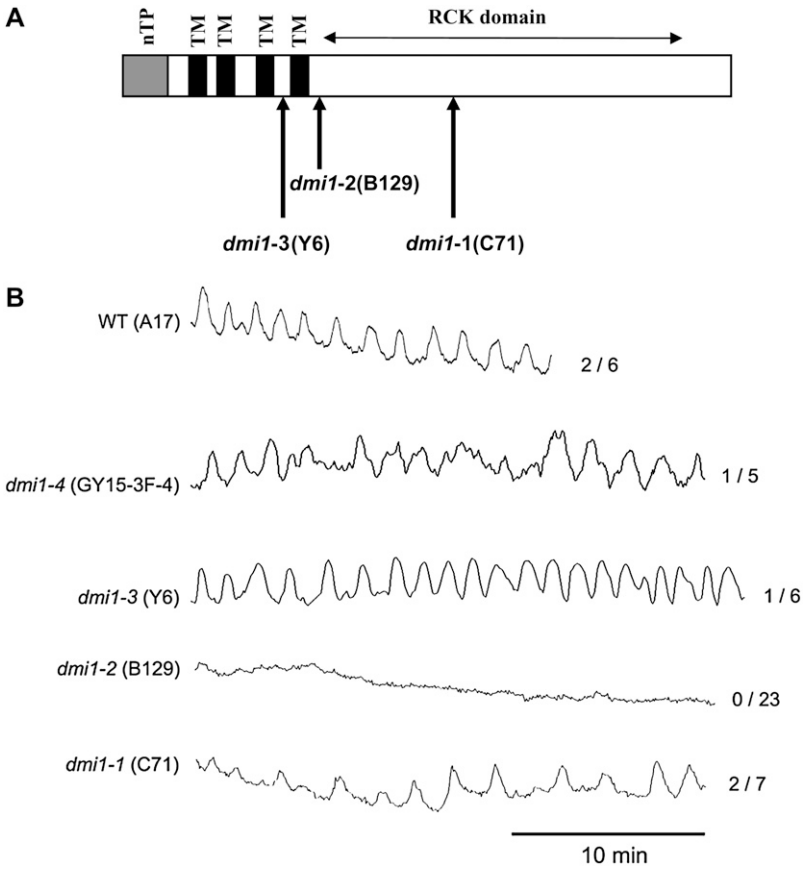

Figure 1. A, Schematic structure of the DMI1 protein and relative position of the stop codons in the *dmi1-1*, *dmi1-2*, and *dmi1-3* alleles. The *dmi1-4* allele contains a complete deletion of the 5′ end of the gene. TM, Transmembrane domain; nTP, nuclear targeting peptide as demonstrated by Riely et al. (2007). B, The *dmi1-2* mutant allele is defective in Mas7-induced Ca^{2+} spiking. Cells of wild-type and mutant lines were microinjected with the Ca^{2+}-responsive dye Oregon green and the nonresponsive dye Texas red. Ca^{2+} changes were measured as the ratio of Oregon green to Texas red, allowing pseudoratiometric imaging of Ca^{2+} changes in Mas7-treated cells. The *y* axis represents the ratio of Oregon green to Texas red in arbitrary units. Representative traces are shown. The numbers indicate the numbers of Mas7-responsive cells per total number of cells analyzed.

et al., 1996). As Li^+ can affect the same molecular targets as Na^+, sensitivity to both ions is commonly linked (Murguia et al., 1995). Figure 3A shows that expression of the full-length *DMI1* cDNA in the G19 mutant resulted in a further increase of Na^+ and Li^+ sensitivity of this strain. The increased Na^+ sensitivity was not due to osmotic effects because the *DMI1*-expressing G19 was not more sensitive to 400 mM K^+ or 800 mM mannitol (data not shown). DMI1 also increased the Li^+ sensitivity of the wild-type strain W303 (data not shown).

Given our interpretation that the *dmi1-2* allele acts in a dominant-negative manner in planta, we tested the effect of *dmi1-2* cDNA expression on Li^+ and Na^+ sensitivity of yeast. As shown in Figure 3A, Li^+ sensitivity, and to a lesser extent Na^+ sensitivity, of the G19 strain were decreased in *dmi1-2* transformants. This provides further evidence that the dmi1-2 protein is partially functional and suggests that dmi1-2 acts opposite to wild-type DMI1.

The decreased Li^+/Na^+ sensitivity of the *dmi1-2*-expressing yeast is difficult to reconcile with a location of this protein in the yeast plasma membrane. Moreover, we observed that Na^+ accumulation from medium containing 10 to 200 mM Na^+ was not affected by *DMI1* expression (Fig. 3B), which suggests that *DMI1* does not alter Li^+/Na^+ conductance in the yeast plasma membrane. Thus, DMI1 may affect the internal sensitivity of yeast cells to Li^+ and Na^+.

Table I. *Hairy root complementation tests for nodulation with M. truncatula DMI1*

Plant Background	Transforming Binary Plasmid	Transformed GUS Plants	No. of Plants Nodulated
dmi1-2	pCAMBIA-1303 (empty vector)	36	0
dmi1-2	pCAMBIA-DMI1	62	44
dmi1-4	pCAMBIA-DMI1	25	22

DMI1 Localizes to the ER in Yeast

To localize DMI1 in yeast we first constructed C- and N-terminal fusions of DMI1 with GFP. Yeast cells expressing *DMI1*::*GFP* or *GFP*::*DMI1* showed a punctate pattern of GFP fluorescence in the cytoplasm (data not shown). However, neither construct produced the Na^+- or Li^+-hypersensitive phenotypes observed in *DMI1*-expressing G19 yeast, indicating the fusion proteins were either alternatively targeted or not functional (data not shown). Therefore we localized DMI1 by indirect immunofluorescence microscopy. Probing of fixed, permeabilized *DMI1*-expressing yeast cells with an antiserum raised against N-terminal peptides of DMI1 stained the yeast cells in an ER-like pattern (Fig. 4, A and B). Fluorescence was absent in vector

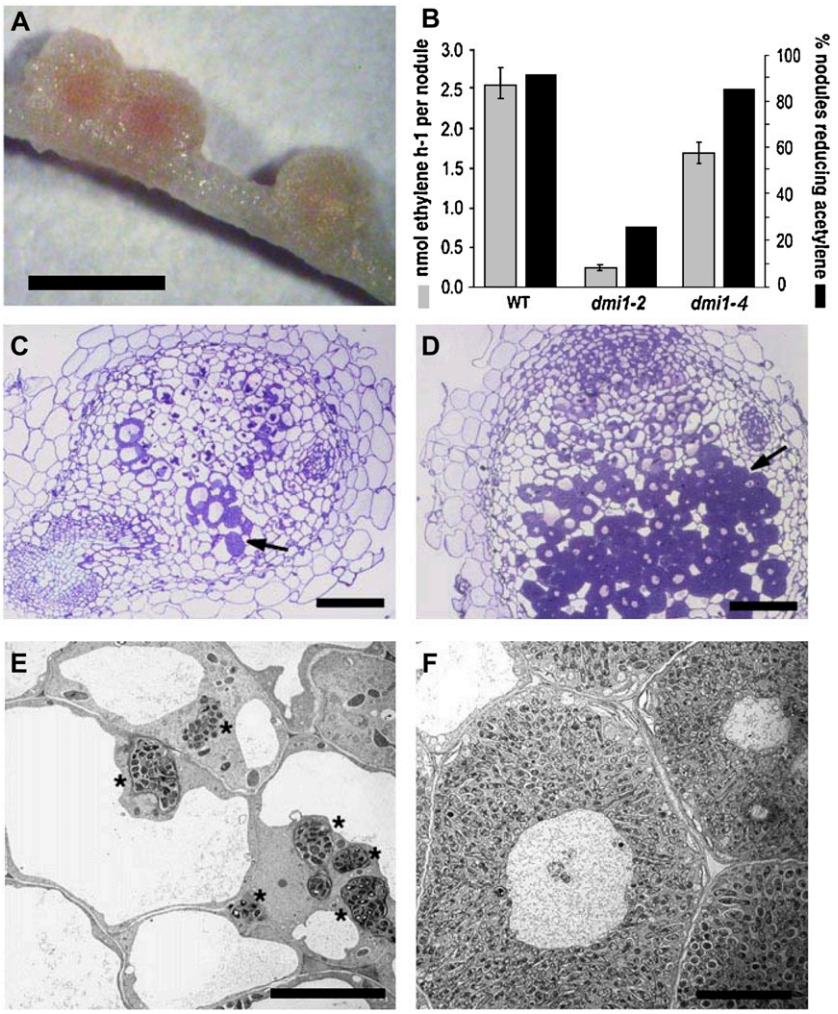

Figure 2. The dmi1-2 protein interferes with DMI1 during nodule development. A, Complemented *dmi1-2* mutants produce small pink and white nodules after 21 d. B, Acetylene reduction assays (light bars) show that the complemented *dmi1-2* nodules have much lower nitrogenase activity than the complemented *dmi1-4* nodules. Additionally, the percentage of complemented *dmi1-2* nodules that reduce acetylene (dark bars) is much lower compared to the complemented *dmi1-4* nodules. C, Light micrograph of a white, nonfixing complemented *dmi1-2* nodule section. D, Light micrograph of a pink, nitrogen-fixing complemented *dmi1-2* nodule section. Within the white nodules, a very low infection rate is observed (C), whereas the pink nodules show many infected cells (arrow in D). E and F, Transmission electron micrographs of complemented *dmi1-2* nodules. E. White, nonfixing nodule showing several swollen infection threads containing bacteria (*). F. Pink, fixing nodule showing normally infected cells packed with bacteroids. Bars: 1 mm (A), 0.2 mm (C and D), and 10 μm (E and F).

control cells (data not shown). The precise localization of DMI1 in yeast was determined by immunogold electron microscopy of high pressure frozen/freeze substituted yeast cells, a method that maintains the integrity of subcellular compartments and sample antigenicity. As shown in Figure 4D, immunogold label was most prominent along the ER and to a lesser degree at the nuclear envelope, consistent with the immunofluorescence observations (Fig. 4B) and reflecting the continuity of these two compartments. In control cells, weak background labeling was observed on cell walls and in vacuoles, but notably absent from the ER and nuclear envelope (Fig. 4C).

Wild-Type *DMI1* and the *dmi1-2* Allele Affect the Hexose-Induced $[Ca^{2+}]_{cyt}$ Transient in Yeast

We hypothesized that DMI1 might exacerbate Li^+ sensitivity by interfering in a $[Ca^{2+}]_{cyt}$-dependent pathway. To examine $[Ca^{2+}]_{cyt}$ responses, we transformed the yeast strains with an *APOAEQUORIN*-carrying plasmid (Batiza et al., 1996). After aequorin reconstitution by incubation with coelenterazine, $[Ca^{2+}]_{cyt}$-dependent light emission was detected by luminometry and $[Ca^{2+}]_{cyt}$ was calculated from photon counts (Allen et al., 1977). Addition of Gal to mid-log phase cultures starved of the sugar for 2.5 h produced a $[Ca^{2+}]_{cyt}$ transient which peaked approximately 5 min after injection (Fig. 5A, black trace). Addition of Glc produced a similar $[Ca^{2+}]_{cyt}$ response (data not shown). In accordance with published data (Csutora et al., 2005), the presence of 10 mM Li^+ during the starvation period diminished the Gal-induced $[Ca^{2+}]_{cyt}$ transient (Fig. 5A, red trace). Addition of Li^+ immediately prior to Gal readdition did not affect the $[Ca^{2+}]_{cyt}$ response, indicating that Li^+ was not likely to act on the Ca^{2+} channel itself (data not shown).

To determine the source of the Gal-induced $[Ca^{2+}]_{cyt}$ transient, we depleted the medium of Ca^{2+} by adding the pH-insensitive Ca^{2+} chelator 1,2-bis(2-aminophenoxy)ethane-*N*,*N*,*N*′,*N*′-tetraacetic acid (BAPTA). Figure 5B shows that the $[Ca^{2+}]_{cyt}$ transient was not decreased, and was even accelerated, by

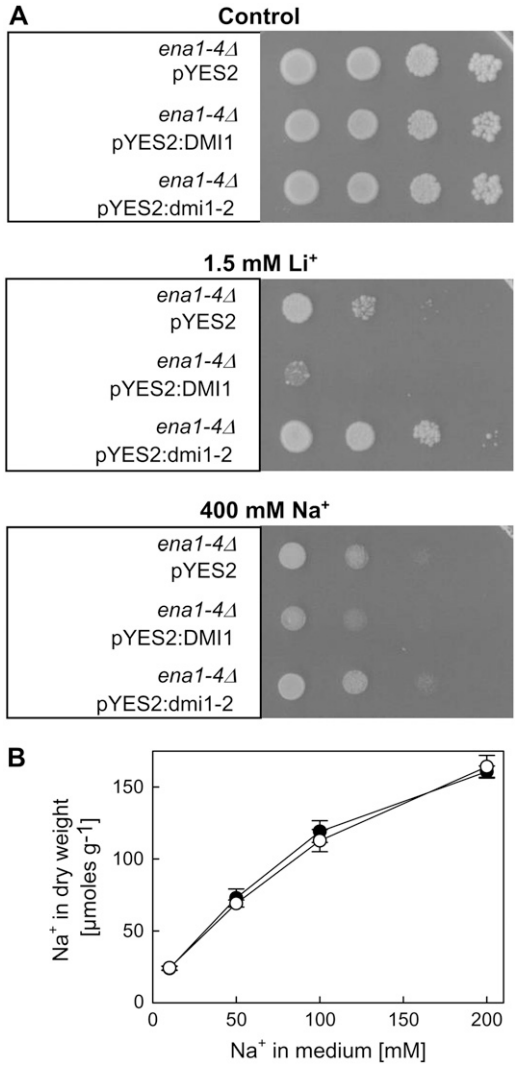

Figure 3. DMI1 and dmi1-2 mutant proteins alter Li^+ and Na^+ sensitivity of the G19 (*ena1-4Δ*) yeast strain. A, Drop assays. Log-phase yeast cultures (1×10^7 cells mL^{-1}) were diluted 10, 100, and 1,000-fold, and spotted onto SC (Gal) agar plates containing the indicated concentrations of Na^+ or Li^+. Drop assays were repeated three times with similar results. B, Na^+ accumulation assay. G19 yeast transformed with pYES2 (black circles) or pYES2:DMI1 (white circles) was grown in SC (Gal) medium containing the indicated concentrations of Na^+. Data are the means ± SEM of three independent experiments.

addition of 10 mM BAPTA. This indicates that the Gal-induced $[Ca^{2+}]_{cyt}$ elevation is primarily derived from internal stores. To determine the identity of this compartment we analyzed a *pmr1*Δ mutant for this response. *PMR1* encodes a Ca^{2+}/Mn^{2+}-ATPase localized in the medial Golgi (Antebi and Fink, 1992; Dürr et al., 1998). *pmr1*Δ mutants have strongly decreased $[Ca^{2+}]$ levels in the ER (Strayle et al., 1999) and an increased steady-state $[Ca^{2+}]_{cyt}$ (Halachmi and Eilam, 1996). The Gal-induced $[Ca^{2+}]_{cyt}$ transient was almost completely abolished in the *pmr1*Δ mutant (Fig. 5C, red trace), whereas its parental strain responded similarly to the G19 mutant (Fig. 5C, black trace). This indicates that the source of the Gal-induced $[Ca^{2+}]_{cyt}$ transient is a PMR1-dependent store, i.e. the ER or the Golgi apparatus. Notably, the ER is also the site where we localized DMI1.

To examine whether DMI1 affects the Gal-induced $[Ca^{2+}]_{cyt}$ transient, we performed luminometric experiments on *DMI1*-expressing cells. Strikingly, the $[Ca^{2+}]_{cyt}$ transient was abolished in *DMI1* transformants (Fig. 5D, black trace). Instead, cells responded with a less pronounced $[Ca^{2+}]_{cyt}$ elevation that was maintained for at least 20 min. The same response was observed if Glc was added to the starved cells (data not shown). This altered $[Ca^{2+}]_{cyt}$ response was also decreased by Li^+ pretreatment (Fig. 5D, red trace). These results demonstrate that Li^+ and DMI1 additively interfere with the Gal-induced $[Ca^{2+}]_{cyt}$ signal. The altered $[Ca^{2+}]_{cyt}$ response of the *DMI1*-expressing strain was accompanied by a growth defect: After 14 h of hexose starvation followed by Gal addition, the empty vector strains started regrowth without a lag phase, whereas growth was delayed for several hours in the *DMI1* transformants (Supplemental Fig. S2). We hypothesize that the hexose-induced $[Ca^{2+}]_{cyt}$ transient is required for an efficient adaptation to altered supply of the energy source.

The hexose-related phenotypes of *DMI1*-expressing cells suggest that the effect of DMI1 on $[Ca^{2+}]_{cyt}$ is independent of Li^+ and Na^+. However, standard synthetic complete (SC) medium contains 1.7 mM Na^+, and the aequorin experiments were carried out with a Na^+/Li^+ efflux-deficient yeast mutant, leaving open the possibility that DMI1 conducts Na^+ to a sensitive compartment, thereby altering $[Ca^{2+}]_{cyt}$ dynamics. Therefore, we grew *DMI1*- and empty vector-transformed wild-type yeast strains (W303-1A) for several generations in Na^+-depleted SC medium (prepared from ultrapure salts without Na^+). Under these conditions, DMI1 had the same effect on the hexose-induced $[Ca^{2+}]_{cyt}$ transient as it had on G19 cells grown in standard SC medium (Fig. 5E). These results show that the DMI1 effect on $[Ca^{2+}]_{cyt}$ homeostasis is independent of Li^+ or Na^+.

If both Na^+/Li^+ sensitivity and alteration of the hexose-induced $[Ca^{2+}]_{cyt}$ transient are due to the same action of DMI1, then the *dmi1*-2 mutant allele might alter the hexose-induced $[Ca^{2+}]_{cyt}$ transient in a way different to that of *DMI1*. To test this possibility, we measured the kinetics of the Gal-induced $[Ca^{2+}]_{cyt}$ transient in yeast cells expressing *dmi1-2*. As shown in Figure 5F, the maximum amplitude of the $[Ca^{2+}]_{cyt}$ transient did not differ between the vector control and *dmi1-2*-transformed strains. However, return of $[Ca^{2+}]_{cyt}$ to the steady-state level was significantly delayed in the *dmi1-2* transformant. Thus, wild-type DMI1 and truncated dmi1-2 affect the kinetics of the hexose-induced $[Ca^{2+}]_{cyt}$ transient differentially. Moreover, these Ca^{2+} phenotypes are independent of Li^+ and Na^+. Taken together, these results suggest that the altered Li^+/Na^+ sensitivity associated with DMI1

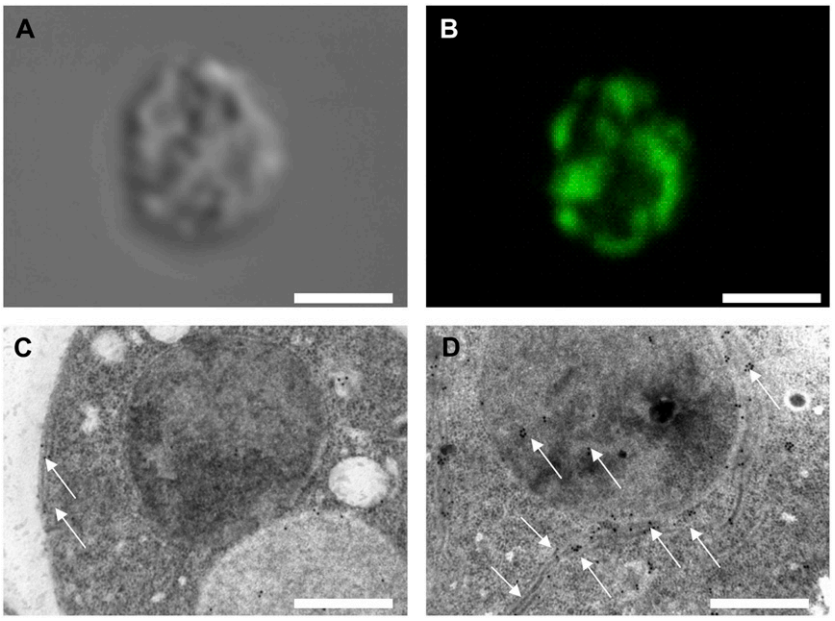

Figure 4. DMI1 localizes to the ER in yeast. A and B, Localization of DMI1 in a G19 yeast cell by indirect immunofluorescence microscopy. Yeast cells were fixed, permeabilized, and labeled with a DMI1-specific antibody and a fluorescent secondary antibody as described in "Materials and Methods." A, Differential interference contrast image. B, Corresponding fluorescence image. C and D, Localization of DMI1 in a G19 yeast cell by immunogold labeling (arrows). C, Vector-only control cell showing some background signal mainly at the cell wall and the vacuole. D, DMI1-transformed cell showing strong labeling of the ER. Some signal is also observed on the nuclear envelope. Bars: 5 μm (A and B) and 0.5 μm (C and D).

and dmi1-2 is mediated by an effect on $[Ca^{2+}]_{cyt}$ homeostasis.

DISCUSSION

The aim of this study was to investigate further the role of DMI1 in Nod factor signaling by combining mutant analysis in planta with bioassay of ion homeostasis in the heterologous yeast system. DMI1 is required for the generation of Nod factor-induced, nucleus-associated Ca^{2+} spikes that are critical for nodule initiation. Ca^{2+} oscillations and related downstream transcriptional responses can also be induced by the G-protein agonist Mastoparan. Interestingly, sensitivity of plant gene expression to Mastoparan is retained in *dmi1* null mutants, putting the role of DMI1 in the Ca^{2+} oscillatory machinery into question. This study provides direct evidence that DMI1 is able to regulate the release of Ca^{2+} from internal stores, both in the model legume *M. truncatula* and in yeast.

dmi1-2, a Semidominant-Negative Allele

Our Ca^{2+} imaging experiments show that, unlike other *dmi1* mutant alleles, the *dmi1-2* allele fails to elicit the Mas7-induced Ca^{2+} response, suggesting that dmi1-2 interferes with Ca^{2+} channel activation. This mutant allele also interferes with the development of functional (nitrogen-fixing) nodules following complementation with the wild-type *DMI1* gene. Taken together, these observations suggest a direct role of DMI1 in both Nod factor-induced Ca^{2+} spiking and late nodule development. In complemented roots, *dmi1-2* interferes with the release of bacteria from infection threads and this appears to result in enlarged and swollen infection threads inside nodules. Interestingly, DMI2 has been shown to have an analogous role in bacterial release, and plants with reduced levels of *DMI2* show a similar phenotype to what we observed in complemented *dmi1-2* plants: limited bacterial release and swollen infection threads inside nodules (Limpens et al., 2005). Thus, our work provides additional support for the hypothesis that Nod factor signal transduction is necessary at both early and late stages of the interaction between legumes and rhizobia.

The *dmi1-2* gene product lacks the entire cytosolic C terminus, including the RCK domain. In the bacterial potassium channel MthK, the RCK domain regulates channel activity in response to Ca^{2+} or other ligands, such as NAD (Jiang et al., 2002). We hypothesize that the dmi1-2 protein forms a deregulated channel subunit that may affect the activity of other channels (see below). This is supported by our yeast experiments. Whereas DMI1 suppresses a hexose-induced Ca^{2+} transient in yeast (and this is correlated with enhanced sensitivity to Na^+ and Li^+), the expression of *dmi1-2* in yeast has the opposite effect, extending the hexose-induced Ca^{2+} transient and increasing resistance to high concentrations of Na^+ and Li^+. The fact that *dmi1-2* had opposite effects to *DMI1* in yeast is also a strong indication that the unusual effects of *dmi1-2* in *M. truncatula* are due to this allele rather than occasional second-site mutations that might persist in the backcrossed *dmi1-2* line. Although the initial description of *dmi1* mutants describes *dmi1-2* as a recessive allele (Catoira et al., 2000), this characterization was based on a presence/absence scoring of nodule structures, without cytological or biochemical analysis of nodule structure or function in heterozygous plants. Our observations indicate that the *dmi1-2* allele has a dominant-negative nature in plants and that the penetrance of the *dmi1-2* phenotype is likely to depend on the relative concentration of mutant versus wild-type

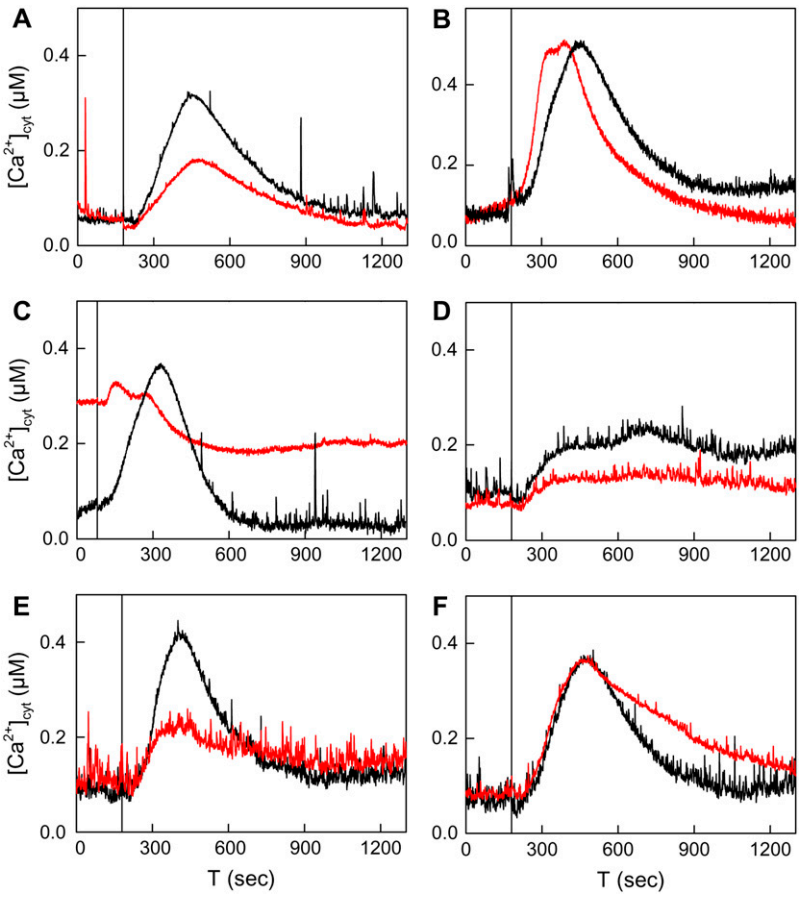

Figure 5. The Gal-induced $[Ca^{2+}]_{cyt}$ transient in yeast is Li^+ sensitive, originates mainly from internal stores, and is altered by *DMI1* and *dmi1-2*. Log-phase *APOAEQUORIN*-expressing cultures were starved for 2.5 h in hexose-free SC medium. At the indicated time points an equal volume of SC medium containing 2% Gal was injected. $[Ca^{2+}]_{cyt}$ was recorded by luminometry. A, G19 pYES2 yeast was starved in medium containing no LiCl (black trace) or 10 mM LiCl (red trace) prior to Gal resupply. B, Ten millimolar BAPTA (red trace) or hexose-free medium only (black trace) were added to starved W303 pYES2 yeast at −10 min. Cells were resupplied with SC (Gal) medium containing 10 mM BAPTA (red trace) or no BAPTA (black trace). C, Response of the *pmr1*Δ pYES2 mutant (red trace) and its parental strain BY4741 pYES2 (black trace) to Gal resupply. D, G19 pYES2:DMI1 yeast was starved in medium containing no LiCl (black trace) or 10 mM LiCl (red trace). E, W303 pYES2 (black trace) and W303 pYES2:DMI1 (red trace) strains were precultured and starved in Na^+-depleted media. F, Response of W303 pYES2 (black trace) and W303 pYES2:dmi1-2 (red trace) to Gal resupply.

protein. We suggest that the hairy root complementation assays of endogenous *dmi1-2* by ectopic *DMI1* yield ratios of the two protein forms that are well suited for producing the intermediate nodulation phenotype observed in Figure 2.

The dominant-negative nature of the *dmi1-2* allele is likely due to the formation of multimers between DMI1 and dmi1-2. Cation channels homologous to DMI1 (e.g. MthK) consist of four pore-forming subunits (Jiang et al., 2002), and an identical structure is to be expected for DMI1. Heteromers consisting of DMI1 and dmi1-2 subunits are likely to be defectively regulated, because their gating ring is incomplete. Dosage-dependent negative dominance of a cation channel mutation in plants has also been demonstrated for the tetrameric Shaker-like K^+ channel KAT1 (Kwak et al., 2001).

DMI1 Effects on Na^+/Li^+ Sensitivity and Ca^{2+} Signaling in Yeast

Expression of *DMI1* and *dmi1-2* in yeast resulted in increased and decreased Na^+/Li^+ sensitivity, respectively. The Na^+ accumulation data and the localization of DMI1 to yeast ER and nuclear membranes argue in favor of a model wherein DMI1 alters the sensitivity to intracellular Na^+/Li^+ in yeast, rather than altering Na^+/Li^+ accumulation. Li^+ effects have been extensively studied in mammals, and to some extent also in yeast. In mammals, Li^+ inhibits glycogen synthase kinase-3 and inositol phosphatases. Inhibition of the latter causes a disruption of the inositol cycle and thereby decreased levels of cellular $InsP_3$ and disturbances in $[Ca^{2+}]_{cyt}$ signaling (Williams and Harwood, 2000). Inositol phosphatase homologs in plants and yeast have also been demonstrated to be sensitive to Li^+, and to a lesser extent also to Na^+ (Murguia et al., 1995; Quintero et al., 1996; Lopez et al., 1999). The yeast genes *IMP1* and *IMP2* encode Li^+- and Na^+-sensitive inositol monophosphatases (Lopez et al., 1999). Deletion of *imp1* and *imp2* causes a drop in $InsP_3$ levels by 60% and Li^+ treatment of wild-type yeast has a similar effect (Navarro-Avinó et al., 2003). Conversely, overexpression of the yeast inositol monophosphatases increases $InsP_3$ levels and raises the steady-state $[Ca^{2+}]_{cyt}$ of yeast cells (Lopez et al., 1999; Navarro-Avinó et al., 2003). Interestingly, there is convincing evidence for an essential role of $InsP_3$ in hexose sensing of yeast (although $InsP_3$-activated channels have not been identified): Readdition of Glc to starved cells induces a transient rise in cellular $InsP_3$, followed by a transient $[Ca^{2+}]_{cyt}$ elevation (Tisi et al., 2004). Phospholipase C is absolutely required for this hexose-induced $[Ca^{2+}]_{cyt}$ transient and the response is augmented in strains deficient in $InsP_3$ phosphorylation (Tisi et al., 2002, 2004). In agreement with a critical role of the inositol cycle in hexose sensing, Li^+ has been shown to

affect the hexose-induced $[Ca^{2+}]_{cyt}$ transient (Csutora et al., 2005). However, this may also be attributed to the inhibition of phosphoglucomutase (PGM), a further Li^+-sensitive yeast enzyme that is also required for the hexose-induced $[Ca^{2+}]_{cyt}$ response (Fu et al., 2000; Masuda et al., 2001).

Irrespective of the primary Li^+ target, it is most likely that Li^+ sensitivity in yeast is at least partially due to disturbances in $[Ca^{2+}]_{cyt}$ signaling and that DMI1 and dmi1-2 also interfere in this signaling network. The results of our luminometric assays clearly support such a notion. We demonstrate that DMI1 inhibits and dmi1-2 prolongs the hexose-induced $[Ca^{2+}]_{cyt}$ transient that originates from a store dependent on Pmr1, a Ca^{2+} pump known to supply the Golgi and ER compartments. One possible mechanism for the inhibition of the $[Ca^{2+}]_{cyt}$ transient by DMI1 might be a continuous depletion of $[Ca^{2+}]_{ER}$ by DMI1 channel activity. However, this is unlikely because yeast mutants with depleted $[Ca^{2+}]_{ER}$ (e.g. *pmr1*Δ, Fig. 5C) have an increased $[Ca^{2+}]_{cyt}$ due to the activation of store-operated Ca^{2+} channels in the plasma membrane (Locke et al., 2000), whereas steady-state $[Ca^{2+}]_{cyt}$ is not increased in *DMI1*-expressing strains. Alternatively, DMI1 might inhibit Li^+-sensitive PGM. This is also unlikely, because *pgm* deletion strains hyperaccumulate Ca^{2+}, which is not observed in *DMI1*-expressing strains (data not shown). The most likely scenario of DMI1 action is an interference of DMI1 in the activation of the Ca^{2+} channel stimulated by hexose resupply. This could be brought about by direct physical interaction of DMI1 with this channel or by DMI1 channel activity causing an alteration in membrane potential. Both mechanisms would require the presence of DMI1 and the hexose-stimulated channel in the same membrane, which agrees with our experimental data. We currently favor the latter hypothesis, i.e. DMI1 altering the membrane potential, because it does not rely on specific interactions of phylogenetically distant yeast and plant proteins. The inability of dmi1-2 to inhibit the hexose-induced $[Ca^{2+}]_{cyt}$ response indicates that the C terminus of the protein is required for this effect. In *dmi1-2*-expressing cells, the return of $[Ca^{2+}]_{cyt}$ to steady-state levels after hexose stimulation is significantly delayed. This effect obviously does not require the C terminus of the protein and is likely to be equivalent to the prolonged elevation of $[Ca^{2+}]_{cyt}$ in *DMI1*-expressing cells. It is tempting to speculate that the DMI1/dmi1-2-dependent posttransient $[Ca^{2+}]_{cyt}$ elevation is due to channel activity of the full-length or the truncated DMI1 proteins. In support of this idea, a mammalian homolog of DMI1, BKCa, has been demonstrated to be still conductive after removal of its entire C terminus (Piskorowski and Aldrich, 2002).

CONCLUSION

Nod factors induce rapid changes in both Ca^{2+} concentration and gene expression. Mutations and inhibitors that abolish Nod factor-induced Ca^{2+} spiking block gene induction, indicating a specific role for Ca^{2+} spiking in signal transduction. The duration and number of Ca^{2+} spikes is critical for Nod factor-induced *ENOD11* expression in root hair cells (Miwa et al., 2006). A number of genes have been defined that are necessary for Nod factor-induced Ca^{2+} spiking, including the putative cation channel DMI1. This protein localizes to the nuclear envelope of *M. truncatula* root hair cells and this localization correlates with the nuclear association of Ca^{2+} spiking. We have shown previously that *DMI1* is not necessary for Mas7-induced Ca^{2+} oscillations, which appear to mimic Nod factor-induced Ca^{2+} spiking (Sun et al., 2007). Here we demonstrate that *dmi1-2*, a dominant-negative allele, can interfere with Mas7-induced Ca^{2+} spiking. This suggests that DMI1 is not the channel responsible for the oscillatory Ca^{2+} response, but instead that DMI1 may act at a level close to that of Mas7 in the Nod factor signaling cascade. Our work in yeast indicates that DMI1 interferes with the release of Ca^{2+} from ER stores, which normally supply hexose-induced Ca^{2+} transients. It is interesting to note that in both Nod factor-induced Ca^{2+} spiking and hexose-induced $[Ca^{2+}]_{cyt}$ transients the Ca^{2+} signal is dependent on phospholipid signaling. We propose that DMI1 is not the Ca^{2+} channel responsible for Ca^{2+} oscillations, but rather that DMI1 regulates these channel(s), perhaps by mobilizing an as yet undefined cation and thereby altering the membrane potential. The localization of DMI1 to the ER membrane in yeast and nuclear membrane in plants complicates a direct electrophysiological analysis of DMI1. Nevertheless, analysis of mutant alleles, such as those employed here, offer insight into the mode of action of DMI1. Similar structure-function analyses should provide novel insights into the activation of Ca^{2+} oscillations in plant systems.

MATERIALS AND METHODS

Plant Material and Growth Methods

Medicago truncatula lines used were Jemalong A17 and homozygous lines of the *dmi1-2* and *dmi1-4* mutants that had been backcrossed once. Seeds were scarified in concentrated sulfuric acid for 8 min, surface sterilized in 12% sodium hypochlorite, imbibed in sterile water, and plated on 1% deionized water agar plates. Seeds were subsequently stratified for 24 or 48 h at 4°C and germinated by incubating at room temperature overnight. All nodulation assays were performed using a suspension of approximately 10^7 cfu mL^{-1} of *Sinorhizobium meliloti* strain ABS7M (pXLGD4) as described previously. For Ca^{2+} imaging, seedlings were grown overnight on buffered Nodulation Agar medium at pH 6.5 (Erhardt et al., 1996) containing the ethylene inhibitor L-α-(2-aminoethoxyvinyl)-Gly (0.1 μM) at 25°C, with the roots shaded by wrapping the plates in aluminum foil.

Agrobacterium rhizogenes (QUA1; Quandt et al., 1993) carrying pCAMBIA-1303 or pCAMBIA-DMI1 (Ané et al., 2004) was used for *M. truncatula* hairy root transformation (Boisson-Dernier et al., 2001). Following transformation, seedlings were grown for 3 weeks and then transferred to CYG growth pouches (16.5 cm × 17.5 cm; Mega International) and inoculated with *S. meliloti* strain 1021/pXLD4. Nodulation was scored after 21 d. pCAMBIA-1303 carries *uidA* under the 35S promoter and this was used to identify transformed roots as described by Jefferson (1987). Acetylene reduction measurements

were carried out on 21-d-old nodules as described by Somasegaran and Hoben (1994). Results were expressed as nanomoles ethylene produced per hour per nodule. Nodules were cut in half longitudinally and fixed, sectioned, and stained as described previously in Lodwig et al. (2005).

DMI1 Expression Analysis

Root samples were collected from 7-d-old *M. truncatula* seedlings grown on Fahraeus medium. Total RNA was extracted using QIAGEN RNeasy plant mini kit. DNA contamination was removed using Ambion's DNA-free kit and total RNA was quantified using RiboGreen RNA quantification kit (Molecular Probes/Invitrogen). A total of 0.5 μg of RNA was used to synthesize cDNA, using oligo dT primers with SuperscriptIII cDNA synthesis kit of Invitrogen. The primers 5′-ATCTTCTATCTTTTAGTTATCTGTTG-3′ and 5′-CAAAAGTGAGCCCAATTTGTCACTCC-3′ were used for *DMI1* and 5′-TGGCATCACTCAGTACCTTTCAACAG-3 and 5′-ACCCAAAGCATCAAATAATAAGTCAACC-3′ for *MtActin2*. A standard reverse transcription-PCR procedure was followed as described in Ané et al. (2004).

Calcium Imaging in *Medicago* Root Hairs

For the Ca^{2+} analysis we microinjected root hair cells with Ca^{2+}-responsive dyes as described by Erhardt et al. (1996), with slight modifications as described by Wais et al. (2000). Micropipettes were pulled from filamented capillaries on a pipette puller (model 773, Campden Instruments). These were loaded with the Ca^{2+}-responsive dye Oregon green dextran (10,000 MW; Invitrogen) and the nonresponsive dye Texas red dextran (10,000 MW; Invitrogen). Injections were performed using iontophoresis with currents generated from a cell ampliflier (model Intra 767, World Precision Instruments) and a stimulus generator made to our specifications (World Precision Instruments). Cells were analyzed on an inverted epifluorescence microscope (model TE2000, Nikon) using a monochromator (Optoscan, Cairn Research) to generate specific wavelengths of light. During image capture the image was split using an Optosplit (Cairn Research), and each image passed through a filter for either Oregon green or Texas red emissions prior to exposure on the CCD chip (ORCA-ER, Hamamatsu). The data was analyzed using Metafluor software (Molecular Devices).

Yeast Strains, Plasmids, and Growth Methods

The yeast (*Saccharomyces cerevisiae*) deletion mutant Y04534 (*pmr1*Δ; *MAT***a**; *his3*Δ*1*; *leu2*Δ*0*; *met15*Δ*0*; *ura3*Δ*0*; *YGL167c*::*kanMX4*) and its parental strain BY4741 (*MAT***a**; *his3*Δ*1*; *leu2*Δ*0*; *met15*Δ*0*; *ura3*Δ*0*) were obtained from the Euroscarf collection (Winzeler et al., 1999). The salt-sensitive yeast strain G19 [*ena1*Δ-*ena4*Δ; *MAT***a**, *leu2-3*, *2-112*, *trp1-1*, *ura3-3*, *ade2-1*, *his3-11*, *can1-100*, *15*(ϕ), *ena1*::*HIS3*::*ena4*] and its parental strain W303-1A [*MAT***a**, *leu2-3,2-112*, *trp1-1*, *ura3-3*, *ade2-1*, *his3-11*, *can1-100*, *15*(ϕ)] were kindly provided by Alonso Rodriguez-Navarro (Quintero et al., 1996). The Ca^{2+} channel mutant strain *cch1*Δ*mid1*Δ (*MAT***a**, *leu2-3*, *112*, *his4*, *trp1*, *ura3-52*, *rme1*, *HMLa*, *cch1*::*KanMX*, *mid1*::*KanMX*) was created from its parental strain JK9-3da (*MAT***a**, *leu2-3*, *112*, *his4*, *trp1*, *ura3-52*, *rme1*, *HMLa*) in a previous study (Fischer et al., 1997). The K^+ channel mutant strain PLY246 (*trk1*Δ*trk2*Δ*tok1*Δ; *MAT***a**; *his3*Δ*200*; *leu2-3*,*112 trp1*Δ*901*; *ura3-52*; *suc2*Δ*9*; *trk1*Δ*51*; *trk2*Δ*50*::*lox-kanMX-lox tok1*Δ*1*::*HIS3*) was kindly provided by Hella Lichtenberg-Fraté (Bertl et al., 2003). A *DMI1* cDNA was PCR amplified from wild-type A17 root cDNA using forward and reverse primers containing the *Kpn*I and *Xba*I sites, respectively, and cloned into the pYES2 (Invitrogen) yeast expression vector. This pYES2:DMI1 construct was mutagenized using the QuickChangeII site-directed mutagenesis kit (Stratagene) to mimic the *dmi1-2* mutation. Yeast was transformed with plasmids using a simplified protocol (Elble, 1992). Transformants were selected and maintained on SC agar plates containing 20 g L^{-1} Glc and lacking the appropriate selective markers (Sherman, 2002).

Growth assays on plates and in liquid were performed as described (Peiter et al., 2005a). For drop assays, yeast was grown overnight in selective SC medium containing 20 g L^{-1} Gal to a density of approximately 10^7 cells mL^{-1}, centrifuged, resuspended in sterile water to 1×10^7 cells mL^{-1}, and diluted 10-, 100-, and 1,000-fold. Ten-microliter drops were spotted onto selective SC (Gal) plates. Plates were incubated for 3 to 5 d at 30°C.

Na^+ Accumulation by Yeast

Yeast was grown shaking (180 rpm) at 30°C in SC-Ura (Gal) medium to early stationary phase (approximately 5×10^7 cells mL^{-1}). NaCl was added to 50 mL aliquots as indicated in "Results." After 3 h, cultures were centrifuged (5 min, 3,200*g*, 4°C) and washed twice with 25 mL 10 mM $CaCl_2$ solution at 4°C. Cell densities were determined using a haemacytometer (Improved Neubauer). Pellets were dried at 80°C for 3 d, weighed, and digested in HNO_3 using a microwave accelerated reaction system (Mars 5, CEM). Na^+ concentration in the digests was determined by atomic absorption spectroscopy (Spectr-AA20, Varian).

Production of Polyclonal Antisera

Soluble, tetrameric multiple antigenic peptides corresponding to the DMI1 amino acid sequence 65-FLGIGSTSRKRRQPPPPPSKPPVNLIPPHPR-95 coupled to a trilysine core (Tam, 1988) were synthesized at the Molecular Genetics Instrument Facility at the University of Georgia. Polyclonal, anti-DMI1 antisera were generated in rabbit against this peptide by Chemicon International.

Indirect Immunofluorescence Microscopy of Yeast

Yeast strains were grown overnight in SC-Ura (Gal) medium to a density of approximately 10^7 cells mL^{-1} and fixed by adding one-tenth volume of formaldehyde (37%). Fixed cells were digested, adhered to Teflon-masked polylysine-coated slides, permeabilized, and labeled with primary (1:1,000) and secondary (1:2,000) antibodies following the protocol of Burke et al. (2000). Presence of the primary antibody was detected by labeling with an AlexaFluor488-conjugated donkey anti-rabbit antibody (A21206, Invitrogen). Fluorescence of the secondary antibody was observed using a Zeiss LSM510 confocal laser scanning microscope (488 nm laser line; 505–530 nm band pass emission filter).

Electron Microscopy of Yeast

Soft pellets of yeast cells grown in liquid culture were loaded in sample holders, frozen in a Baltec HPM 010 high-pressure freezer (Technotrade), and then transferred to liquid nitrogen for storage. Freeze substitution was performed in 0.2% uranyl acetate (Electron Microscopy Sciences) plus 0.2% glutaraldehyde (Electron Microscopy Sciences) in acetone at −80°C for 72 h, and warmed to −50°C for 24 h. After several acetone rinses these samples were infiltrated with Lowicryl HM20 (Electron Microscopy Sciences) during 72 h and polymerized at −50°C under UV light for 48 h. Sections were mounted on formvar-coated nickel grids and blocked for 20 min with a 5% (w/v) solution of nonfat milk in phosphate-buffered saline (PBS) containing 0.1% Tween 20. The sections were incubated in the primary anti-DMI1 antibody (1:10 in PBS-Tween 20) for 1 h, rinsed in PBS containing 0.5% Tween 20, and then transferred to the secondary antibody (anti-rabbit IgG 1:50) conjugated to 15 nm gold particles for 1 h. Controls omitted either the primary antibodies or used the preimmune serum.

$[Ca^{2+}]_{cyt}$ Determination in Yeast by Aequorin Luminescence

Yeast strains were transformed with a pEVP11AEQ plasmid carrying the *APOAEQUORIN* gene (Batiza et al., 1996) and maintained on selective SC plates. Aequorin was reconstituted by adding 1 μM coelenterazine (ctz-n; 0.1 mM stock in methanol; Lux Biotechnology) to the yeast culture and incubating for 1 to 2 h at 25°C. Luminescence of 200 μL aliquots was determined using a tube luminometer (Sirius-1, Berthold Detection Systems). After determination of baseline $[Ca^{2+}]_{cyt}$ for 1 min, agents were injected as 2× concentrated stocks in medium. To determine $[Ca^{2+}]_{cyt}$ from luminescence levels, total aequorin was discharged by addition of 500 μL CE solution (2 M $CaCl_2$, 20% ethanol). $[Ca^{2+}]_{cyt}$ values were calculated using the equation derived by Allen et al. (1977). All displayed traces are representative of at least four replicates.

Supplemental Data

The following materials are available in the online version of this article.

Supplemental Figure S1. Expression of *DMI1* does neither restore growth of the *cch1*Δ*mid1*Δ yeast mutant on Ca^{2+}-depleted medium nor growth of the *trk1*Δ*trk2*Δ*tok1*Δ mutant on low-K^+ medium.

Supplemental Figure S2. Expression of *DMI1* delays regrowth of yeast after galactose starvation.

Supplemental Figure S3. Expression levels of *DMI1* and *dmi1-2* in wild-type plants and *dmi1-2* allele, respectively.

ACKNOWLEDGMENTS

We thank Najia Zaman, Sarah Kilmartin, Tina Peiter-Volk, and Sue Bunnewell for their excellent technical support. We are grateful to Alonso Rodriguez-Navarro and Hella Lichtenberg-Fraté for providing the G19 and the PLY246 yeast strains, respectively.

Received January 31, 2007; accepted July 5, 2007; published July 13, 2007.

LITERATURE CITED

Allen DG, Blinks JR, Prendergast FG (1977) Aequorin luminescence: relation of light emission to calcium concentration—a calcium-independent component. Science **195:** 996–998

Allen GJ, Chu SP, Harrington CL, Schumacher K, Hoffmann T, Tang YY, Grill E, Schroeder JI (2001) A defined range of guard cell calcium oscillation parameters encodes stomatal movements. Nature **411:** 1053–1057

Ané JM, Kiss GB, Riely BK, Penmetsa RV, Oldroyd GED, Ayax C, Lévy J, Debellé F, Baek J-M, Kalo P, et al (2004) *Medicago truncatula DMI1* required for bacterial and fungal symbioses in legumes. Science **303:** 1364–1367

Antebi A, Fink GW (1992) The yeast Ca^{2+}-ATPase homologue, PMR1, is required for normal Golgi function and localizes in a novel Golgi-like distribution. Mol Biol Cell **3:** 633–654

Batiza AF, Schulz T, Masson PH (1996) Yeast respond to hypotonic shock with a calcium pulse. J Biol Chem **271:** 23357–23362

Bertl A, Ramos J, Ludwig J, Lichtenberg-Fraté H, Reid J, Bihler H, Calero F, Martinez P, Ljungdahl PO (2003) Characterization of potassium transport in wild-type and isogenic yeast strains carrying all combinations of *trk1*, *trk2* and *tok1* null mutations. Mol Microbiol **47:** 767–780

Boisson-Dernier A, Chabaud M, Garcia F, Bécard G, Rosenberg C, Barker DG (2001) *Agrobacterium rhizogenes*-transformed roots of *Medicago truncatula* for the study of nitrogen-fixing and endomycorrhizal symbiotic associations. Mol Plant Microbe Interact **14:** 695–700

Burke D, Dawson D, Stearns T (2000) Methods in Yeast Genetics. Cold Spring Harbor Laboratory Press, New York

Catoira R, Galera C, de Billy F, Penmetsa RV, Journet E-P, Maillet F, Rosenberg C, Cook D, Gough C, Dénarié J (2000) Four genes of *Medicago truncatula* controlling components of a Nod factor transduction pathway. Plant Cell **12:** 1647–1665

Charron D, Pingret J-L, Chabaud M, Journet E-P, Barker DG (2004) Pharmacological evidence that multiple phospholipid signaling pathways link Rhizobium nodulation factor perception in *Medicago truncatula* root hairs to intracellular responses, including Ca^{2+} spiking and specific *ENOD* gene expression. Plant Physiol **136:** 3582–3593

Csutora P, Strassz A, Boldizsár F, Németh P, Sipos K, Aiello D, Bedwell DM, Miseta A (2005) Inhibition of phosphoglucomutase activity by lithium alters cellular calcium homeostasis and signaling in *Saccharomyces cerevisiae*. Am J Physiol Cell Physiol **289:** C58–C67

Dolmetsch RE, Xu K, Lewis RS (1998) Calcium oscillations increase the efficiency and specificity of gene expression. Nature **392:** 933–936

Dürr G, Strayle J, Plemper R, Elbs S, Klee SK, Catty P, Wolf DH, Rudolph HK (1998) The *medial*-Golgi ion pump Pmr1 supplies the yeast secretory pathway with Ca^{2+} and Mn^{2+} required for glycosylation, sorting, and endoplasmic reticulum-associated protein degradation. Mol Biol Cell **9:** 1149–1162

Elble R (1992) A simple and efficient procedure for transformation of yeasts. Biotechniques **13:** 18–20

Engstrom EM, Erhardt DW, Mitra RM, Long SR (2002) Pharmacological analysis of Nod factor-induced calcium spiking in *Medicago truncatula*: evidence for the requirement of type IIA calcium pumps and phosphoinositide signaling. Plant Physiol **128:** 1390–1401

Erhardt DW, Wais R, Long SR (1996) Calcium spiking in plant root hairs responding to Rhizobium nodulation signals. Cell **85:** 673–681

Felle HH, Kondorosi E, Kondorosi A, Schultze M (2000) How alfalfa root hairs discriminate between Nod factors and oligochitin elicitors. Plant Physiol **124:** 1373–1380

Fischer M, Schnell N, Chattaway J, Davies P, Dixon G, Sanders D (1997) The *Saccharomyces cerevisiae CCH1* gene is involved in calcium influx and mating. FEBS Lett **419:** 259–262

Fu L, Miseta A, Hunton D, Marchase RB, Bedwell DM (2000) Loss of the major isoform of phosphoglucomutase results in altered calcium homeostasis in *Saccharomyces cerevisiae*. J Biol Chem **275:** 5431–5440

Halachmi D, Eilam Y (1996) Elevated cytosolic free Ca^{2+} concentrations and massive Ca^{2+} accumulation within vacuoles, in yeast mutant lacking *PMR1*, a homolog of Ca^{2+}-ATPase. FEBS Lett **392:** 194–200

Imaizumi-Anraku H, Takeda N, Charpentier M, Perry J, Miwa H, Umehara Y, Kouchi H, Murakami Y, Mulder L, Vickers K, et al (2005) Plastid proteins crucial for symbiotic fungal and bacterial entry into plant roots. Nature **433:** 527–531

Jefferson RA (1987) Assaying chimeric genes in plants: the *GUS* gene fusion system. Plant Mol Biol Rep **5:** 387–405

Jiang Y, Lee A, Chen J, Cadene M, Chait BT, MacKinnon R (2002) Crystal structure and mechanism of a calcium-gated potassium channel. Nature **417:** 515–522

Klüsener B, Boheim G, Liß H, Engelberth J, Weiler EW (1995) Gadolinium-sensitive, voltage-dependent calcium release channels in the endoplasmic reticulum of a higher plant mechanoreceptor organ. EMBO J **14:** 2708–2714

Kwak JM, Murata Y, Baizabal-Aguirre VM, Merrill J, Wang M, Kemper A, Hawke SD, Tallman G, Schroeder JI (2001) Dominant negative guard cell K^+ channel mutants reduce inward-rectifying K^+ currents and light-induced stomatal opening in Arabidopsis. Plant Physiol **127:** 473–485

Limpens E, Mirabella R, Fedorova E, Franken C, Franssen H, Bisseling T, Geurts R (2005) Formation of organelle-like N_2-fixing symbiosomes in legume root nodules is controlled by *DMI2*. Proc Natl Acad Sci USA **102:** 10375–10380

Locke EG, Bonilla M, Liang L, Takita Y, Cunningham KW (2000) A homolog of voltage-gated Ca^{2+} channels stimulated by depletion of secretory Ca^{2+} in yeast. Mol Cell Biol **20:** 6686–6694

Lodwig EM, Leonard M, Marroqui S, Wheeler TR, Findlay K, Downie JA, Poole PS (2005) Role of polyhydroxybutyrate and glycogen as carbon storage compounds in pea and bean bacteroids. Mol Plant Microbe Interact **18:** 67–74

Lopez F, Leube M, Gil-Mascarell R, Navarro-Avinó JP, Serrano R (1999) The yeast inositol monophosphatase is a lithium- and sodium-sensitive enzyme encoded by a non-essential gene pair. Mol Microbiol **31:** 1255–1264

Masuda CA, Xavier MA, Mattos KA, Galina A, Montero-Lomelí M (2001) Phosphoglucomutase is an *in vivo* lithium target in yeast. J Biol Chem **276:** 37794–37801

Miwa H, Sun J, Oldroyd GED, Downie JA (2006) Analysis of calcium spiking using a Cameleon calcium sensor reveals that nodulation gene expression is regulated by calcium spike number and the developmental status of the cell. Plant J **48:** 883–894

Muir SR, Sanders D (1997) Inositol 1,4,5-trisphosphate-sensitive Ca^{2+} release across nonvacuolar membranes in cauliflower. Plant Physiol **114:** 1511–1521

Murguia JR, Bellés JM, Serrano R (1995) A salt-sensitive 3′(2′),5′-bisphosphate nucleotidase involved in sulfate activation. Science **267:** 232–234

Navarro-Avinó JP, Bellés JM, Serrano R (2003) Yeast inositol mono- and trisphosphate levels are modulated by inositol monophosphatase activity and nutrients. Biochem Biophys Res Commun **302:** 41–45

Navazio L, Bewell MA, Siddiqua A, Dickinson GD, Galione A, Sanders D (2000) Calcium release from the endoplasmic reticulum of higher plants elicited by the NADP metabolite nicotinic acid adenine dinucleotide phosphate. Proc Natl Acad Sci USA **97:** 8693–8698

Navazio L, Mariani P, Sanders D (2001) Mobilization of Ca^{2+} by cyclic ADP-ribose from the endoplasmic reticulum of cauliflower florets. Plant Physiol **125:** 2129–2138

Oldroyd GED, Downie JA (2004) Calcium, kinases and nodulation signalling in legumes. Nat Rev Mol Cell Biol **5:** 566–576

Peiter E, Fischer M, Sidaway K, Roberts SK, Sanders D (2005a) The *Saccharomyces cerevisiae* Ca^{2+} channel Cch1pMid1p is essential for tolerance to cold stress and iron toxicity. FEBS Lett **579:** 5697–5703

Peiter E, Maathuis FJM, Mills LN, Knight H, Pelloux J, Hetherington AM, Sanders D (2005b) The vacuolar Ca^{2+}-activated channel TPC1 regulates germination and stomatal movement. Nature **434:** 404–408

Pingret J-L, Journet E-P, Barker DG (1998) Rhizobium Nod factor signaling: evidence for a G-protein-mediated transduction mechanism. Plant Cell **10:** 659–672

Piskorowski R, Aldrich RW (2002) Calcium activation of BKCa potassium channels lacking the calcium bowl and RCK domains. Nature **420:** 499–502

Quandt H-J, Pühler A, Broer I (1993) Transgenic root nodules of *Vicia hirsuta*: a fast and efficient system for the study of gene expression in indeterminate-type nodules. Mol Plant Microbe Interact **6:** 699–706

Quintero F, Garciadeblás B, Rodriguez-Navarro A (1996) The *SAL1* gene of Arabidopsis, encoding an enzyme with 3′(2′),5′-bisphosphate nucleotidase and inositol polyphosphate 1-phosphatase activities, increases salt tolerance in yeast. Plant Cell **8:** 529–537

Riely BK, Lougnon G, Ané J-M, Cook DR (2007) The symbiotic ion channel homolog DMI1 is localized in the nuclear membrane of *Medicago truncatula* roots. Plant J **49:** 208–216

Shaw SL, Long SR (2003) Nod factor elicits two separable calcium responses in *Medicago truncatula* root hair cells. Plant Physiol **131:** 976–984

Sherman F (2002) Getting started with yeast. Methods Enzymol **350:** 3–41

Somasegaran P, Hoben HJ (1994) Handbook for Rhizobia. Springer, New York

Strayle J, Pozzan T, Rudolph HK (1999) Steady-state free Ca^{2+} in the yeast endoplasmic reticulum reaches only 10 μM and is mainly controlled by the secretory pathway pump Pmr1. EMBO J **18:** 4733–4743

Sun J, Miwa H, Downie JA, Oldroyd GED (2007) Mastoparan activates calcium spiking analogous to Nod factor-induced responses in *Medicago truncatula* root hair cells. Plant Physiol **144:** 695–702

Tam JP (1988) Synthetic peptide vaccine design: synthesis and properties of a high-density multiple antigenic peptide system. Proc Natl Acad Sci USA **85:** 5409–5413

Tisi R, Baldassa S, Belotti F, Martegani E (2002) Phospholipase C is required for glucose-induced calcium influx in budding yeast. FEBS Lett **520:** 133–138

Tisi R, Belotti F, Wera S, Winderickx J, Thevelein JM, Martegani E (2004) Evidence for inositol triphosphate as a second messenger for glucose-induced calcium signalling in budding yeast. Curr Genet **45:** 83–89

Wais RJ, Galera C, Oldroyd G, Catoira R, Penmetsa RV, Cook D, Gough C, Dénarié J, Long SR (2000) Genetic analysis of calcium spiking responses in nodulation mutants of *Medicago truncatula*. Proc Natl Acad Sci USA **97:** 13407–13412

Walker SA, Viprey V, Downie JA (2000) Dissection of nodulation signaling using pea mutants defective for calcium spiking induced in root hairs by Nod factors and chitin oligomers. Proc Natl Acad Sci USA **97:** 13413–13418

Williams RSB, Harwood AJ (2000) Lithium therapy and signal transduction. Trends Pharmacol Sci **21:** 61–64

Winzeler EA, Shoemaker DD, Astromoff A, Liang H, Anderson K, Andre B, Bangham R, Benito R, Boeke JD, Bussey H, et al (1999) Functional characterization of the *S. cerevisiae* genome by gene deletion and parallel analysis. Science **285:** 901–906